

Impact of strange quark matter nuggets on pycnonuclear reaction rates in the crusts of neutron stars

B. Golf,^{*} J. Hellmers,[†] and F. Weber[‡]

*Department of Physics, San Diego State University,
5500 Campanile Drive, San Diego, California 92182, USA*

(Dated: November 8, 2018)

This paper presents an investigation into the pycnonuclear reaction rates in dense crustal matter of neutron stars contaminated with strange quark matter nuggets. The presence of such nuggets in the crustal matter of neutron stars would be a natural consequence if Witten's strange quark matter hypothesis is correct. The methodology presented in this paper is a recreation of a recent representation of nuclear force interactions embedded within pycnonuclear reaction processes. The study then extends the methodology to incorporate distinctive theoretical characteristics of strange quark matter nuggets, like their low charge-per-baryon ratio, and then assesses their effects on the pycnonuclear reaction rates. Particular emphasis is put on the impact of color superconductivity on the reaction rates. Depending on whether or not quark nuggets are in this novel state of matter, their electric charge properties vary drastically which turns out to have a dramatic effect on the pycnonuclear reaction rates. Future nuclear fusion network calculations may thus have the potential to shed light on the existence of strange quark matter nuggets and on whether or not they are in a color superconducting state, as suggested by QCD.

PACS numbers: 21.65.Qr; 25.60.Pj; 26.50.+x; 97.10.Cv; 97.60.Jd

I. INTRODUCTION

First proposed in 1934 and subsequently observed in 1967, neutron stars are the remnants of supernova explosions of aging supergiant stars. They are extremely massive at approximately 1.4 times the mass of the sun. The interior structure of a neutron star is still the subject of debate, as neutron stars are tremendously compact objects, crushing their mass into a radius of roughly ten kilometers. This makes them some of the densest objects known to man, with core densities possibly more than ten times the density of atomic nuclei. This extreme compression provides a high-pressure environment in which numerous subatomic particle processes are believed to compete with each other and novel phases of matter may exist. The most spectacular ones stretch from the generation of hyperons and baryon resonances [1, 2], to quark deconfinement [3, 4, 5, 6, 7, 8, 9, 10], to the formation of boson condensates [11, 12, 13, 14, 15]. (For overviews, see [1, 2, 16, 17, 18, 19, 20].) It has also been suggested that strange quark matter [21, 22], made up of roughly equal numbers of up, down and strange quarks, may be more stable than ordinary atomic nuclei [26, 27, 28]. This intriguing possibility is known as the strange quark matter hypothesis. In the latter event, neutron stars could be made almost entirely of strange quark matter rather than confined hadronic matter [23, 24, 25]. If quark matter exists in neutron stars it ought to be a color superconductor [29, 30, 31, 32]. This fascinating possibility has renewed

tremendous interest in the physics and astrophysics of quark matter [17, 20, 29, 31, 33].

The idea that quark matter may exist in neutron stars is not new [3, 4, 5, 6, 7, 8, 9]. With the dissolution of nuclei in the cores of neutron stars, the crush of gravity may allow even protons and neutrons to be broken into their constituent components. The baryons at this point exist in such close proximity that their quarks are effectively free. With up and down quarks being the least massive, they would be the first to appear in this deconfined state. Furthermore, given the relatively small mass of the strange quark, it is possible that highly energetic up and down quarks from nucleons may convert to low-energy strange quarks at about the same density [9]. This mixture of up, down, and strange quarks is referred to as strange quark matter if its energy per baryon is less than that of ordinary nuclear matter, as expressed by the strange quark matter hypothesis. Another distinguishing feature between nuclear matter and strange matter is that the latter is self-bound and electrically charge neutral. For that reason strange matter objects can exist stably for a tremendous range of baryon numbers, A , ranging from $\sim 10^2$ to 10^{57} . The low baryon-number end is formed by strangelets (strange nuggets) [21, 34, 35, 36, 37], while the high baryon-number end is populated by strange (quark matter) stars [1, 2, 17, 23, 24, 25].

If strange quark matter exists, it may be present in any of the neutron star regions – in the outer and inner crust through accretion from a companion compact stellar object and in the core through state changes. The base of the outer crust is characterized by a transition known as neutron drip, where the attractive nuclear force that holds subatomic particles together in nuclei is saturated and neutrons subsequently leak out of the nuclei. The in-

^{*}Electronic address: bsouci@gmail.com

[†]Electronic address: hellmersj1@mac.com

[‡]Electronic address: fweber@sciences.sdsu.edu

ner crust is a composite of these free neutrons and a lattice of neutron-rich matter, making this region a suitable environment for the study of high-density nuclear interactions, known as pycnonuclear reactions when a lattice is involved. The lattice structure is a critical feature, as the extreme gravitational force of neutron stars can offset the kinetic and potential energies of the constituent matter in the crust of neutron stars, with the ground state lattice configuration balancing the competing forces. Within this framework, pycnonuclear reactions are distinctive in that they can occur at very low temperatures. In the inner crust, it is possible that pycnonuclear reaction rates between SQM and normal atomic matter may be very different from those between ordinary nuclei. Along this line of inquiry, this is a first step in the examination of pycnonuclear reaction rates between normal nuclear matter and a simple model incorporating some distinct characteristics of strange quark matter.

To this end, the current undertaking recreates recent efforts to quantify pycnonuclear reaction rates, efforts that included ion-ion interaction models systematically constructed from nucleon-nucleon interactions. This study then widens the scope, allowing for the inclusion of theoretical characteristics of strange quark matter. The final encoded methodology calculates rudimentary pycnonuclear reaction rates for different species of inner crust matter in neutron stars, taking basic features of SQM and normal matter and providing reaction rates between them. No assumptions are made about the relative amount of strange quark matter present in the inner crust, beyond postulating its existence; the pycnonuclear reaction calculations are limited to a single primitive lattice cell, with a single strangelet surrounded by normal matter ions. Future work may leverage the magnitude of the differences in reaction rates to modify solar heating models for neutron stars, perhaps providing clarification on the existence of strange quark matter.

The paper is organized as follows. Section II provides an introduction into nuclear reaction rates in high-density environments. The characteristics of strange quark matter that appear to affect the pycnonuclear reaction rates are presented in Section III. This is followed by a review of observed trends and an exploration of possible future work presented in Section IV.

II. PYCNONUCLEAR REACTION RATES

Generally speaking, in pycnonuclear reaction rates, the incoming and target particle densities usually considered in a nuclear reaction are replaced by geometric crystal lattice calculations that account for the separation distance between a specific number of nearby, bound ions. The kinetic energy, usually involving a calculation of the relative velocity, is subsumed in an analysis of the total potential energy of a reacting pair of particles, stemming from both the configuration of the lattice and the vibration of the bound ions. In turn, the incident flux through

a pure coulomb barrier is replaced by an approximate calculation of the wave function transmitted through the total, screened, effective barrier between the two ions.

In a high-density environment, such as a neutron star, it is expected that matter will settle into a low-energy configuration, such as the body-centered cubic which is assumed to have the greatest binding energy per nucleus [38]. The repulsive framework of similarly-charged ions enveloping two reacting ions in a bcc lattice reduces the Coulomb barrier between them, resulting in a barrier potential that is suppressed in both magnitude and range when compared to that denoted by a pure Coulomb law [42]. Since ions trapped in such a lattice will continue to fluctuate about their equilibrium positions in their ground state, the ions may be able to penetrate the Coulomb barrier of a nearby ion [39]. In this effort, consistent with the most common treatment of pycnonuclear reactions within the model of the bcc lattice, the “static lattice” approximation - in which all the surrounding ions as well as the center of mass of the reacting ion pair are considered frozen at their equilibrium positions - is used [40, 41]. Furthermore, the electrons are assumed to act as a background electron gas with a density consistent for charge neutrality, moving within the arrangement of positive charge.

Addressing the units of the reaction rate calculation, lengths and energies for one-component (OCP) and multi-component plasmas (MCP) are usually measured in terms of the characteristic quantities r^* and E^* , respectively. These terms are defined as

$$r_{\text{OCP}}^* = \frac{\hbar^2 4\pi\epsilon_0}{MZ^2e^2}, \quad (1)$$

$$E_{\text{OCP}}^* = \frac{Z^2e^2}{r_{\text{OCP}}^*}, \quad (2)$$

$$r_{\text{MCP}}^* = \frac{A_1 + A_2}{2A_1A_2Z_1Z_2} \frac{\hbar^2 4\pi\epsilon_0}{He^2}, \quad (3)$$

$$E_{\text{MCP}}^* = \frac{Z_1Z_2e^2}{r_{\text{MCP}}^*}, \quad (4)$$

in analogy with the Bohr radius and the ground state energy of an electron in the Bohr model for hydrogen [40]. Here, M is twice the reduced mass for a pair of nuclei, and H is the atomic mass unit in grams. The density of the plasma can then be expressed in terms of r^* and a dimensionless inverse-length parameter λ , introduced by Salpeter and Van Horn in their seminal work on pycnonuclear reactions and defined as

$$\begin{aligned} \lambda_{\text{OCP}} &\equiv r_{\text{OCP}}^* \left(\frac{N_A}{2} \right)^{1/3} \\ &= \frac{1}{AZ^2} \left(\frac{1}{A} \frac{\rho}{1.3574 \times 10^{11} \text{g cm}^{-3}} \right)^{1/3}, \end{aligned} \quad (5)$$

$$\begin{aligned}\lambda_{\text{MCP}} &\equiv r_{\text{MCP}}^* \left(\frac{N_{\text{E}}}{2Z} \right)^{1/3} \\ &= \frac{A_1 + A_2}{2A_1 A_2 Z_1 Z_2 (Z_1 + Z_2)^{1/3}} \\ &\times \left(\frac{\langle Z \rangle}{\langle A \rangle} \frac{\rho}{1.3574 \times 10^{11} \text{ g cm}^{-3}} \right)^{1/3},\end{aligned}\quad (6)$$

where $\langle Z \rangle$ and $\langle A \rangle$ are the mean charge and mean mass number [40, 43].

With respect to the density model that describes the nuclear densities, a two-parameter Fermi (2pF) distribution, or Woods-Saxon potential, is used:

$$\rho(r) = \frac{\rho_0}{1 + \exp\left(\frac{r-R_0}{a}\right)}.\quad (7)$$

The normalization condition is

$$4\pi = \int_0^\infty \rho(r) r^2 dr = X,\quad (8)$$

where X could be the number of protons, neutrons, or nucleons used to determine ρ_0 [45]. This distribution can recreate the saturation of the nuclear medium and the rapid fall-off that brings out the notion of the radius R_0 of the nucleus [45].

On the whole, as an input to the 2pF distributions, the radii of most nuclei are well described by

$$\text{radius (in fermi)} = 1.31 \times A^{1/3} - 0.84,\quad (9)$$

where A is the number of nucleons in a given nucleus [46]. The rapid decrease in density is tied to the diffuseness parameter a . This parameter plays a key role in subsequent models that vary the range of the nuclear force. Both nucleon and matter densities, coupled with their average diffuseness parameters $\bar{a}_{\text{nucleon}} = 0.50$ fm and $\bar{a}_{\text{matter}} = 0.56$ fm, respectively, give similar radii [47].

A. Long-Range Interactions

The constituent calculations of a reaction rate are broken up by where specific forces are dominant, with this factoring into long-range and short-range interactions possible because the lattice separations are much greater than the radii of the ions. As mentioned earlier, calculations for the total kinetic energy involved in normal thermonuclear reactions are replaced by a calculation of the energies of the bound ions in pycnonuclear reactions. Beginning with the electrostatic lattice energy that maintains the structure of the ions, an exact expression for the electrostatic screening potential is available, involving a six-fold sum of the locations of all nearest-neighbor nuclei in the lattice [44]. However, an approximation based on the static lattice paradigm is also possible, reducing the six-fold sum to a triple lattice sum based on the separation distance r between the reacting ion pair. This

approximation leads to the total electrostatic interaction energy per nucleus being given by

$$E_{\text{Coulomb}}^{\text{bcc}} = 1.81962 \frac{Z^2 e^2}{a} = 1.81962 \lambda E^*,\quad (10)$$

where a is a constant of the lattice derived from the baryon number density [44]. However, the lattice energy is not the only energy to consider; the nuclei are also vibrating in their ground states within the bcc lattice. The oscillation frequency of the nuclei around their equilibrium lattice sites is of the order of magnitude of the ion-plasma frequency ω_{p} , defined by [40]

$$\hbar\omega_{\text{p}} = \hbar \left(4\pi \frac{2Z^2 e^2}{a^3 A H} \right)^{1/2} = 2.7426 \lambda^{1/2} E_{\text{Coulomb}},\quad (11)$$

with an anisotropic harmonic oscillator potential describing the relative motion of the two ions. The energy-level spacings for vibrations in the z -axis separating two nearest-neighbor ions in the bcc lattice are [40]

$$\hbar\omega_z = 0.6752 \hbar\omega_{\text{p}}.\quad (12)$$

This vibrational energy in the z -direction along the axis connecting the two reacting nuclei can then be added to the electrostatic energy per particle in the bcc lattice to determine the total energy of the pair-wise nuclear reaction.

To determine the wavefunction of the incoming particle using the total, screened Coulomb potential, Salpeter and Van Horn used a Wentzel-Kramers-Brillouin (WKB) approximation to show that

$$\begin{aligned}\psi(r) &= 0.553 \frac{\lambda^{7/8}}{(r^*)^{3/2}} (r_{\text{n}})^{-1/4} \\ &\times \exp \left[-\frac{1}{2} \lambda^{-1/2} \left(J - \lambda^{1/2} K \right) + 2r_{\text{n}}^{1/2} \right],\end{aligned}\quad (13)$$

with

$$J - \lambda^{1/2} K = 2.638 - 3.6 \lambda^{1/2},\quad (14)$$

is the wave function evaluated at the nuclear radius for the relative motion of the reacting nuclei in the static approximation of the lattice [40]. At this point, all of the long-range interactions for the pair-wise reaction rate W are included, resulting in

$$W = \frac{8 S(E)}{\hbar (r^*)^2} (r^*)^3 r_{\text{n}}^{1/2} \exp \left(4r_{\text{n}}^{-1/2} \right) |\psi_{\text{E0}}(r_{\text{n}})|^2.\quad (15)$$

From here, only the eight nearest-neighbors surrounding any given lattice point are taken into account, resulting in the following expression for the reaction rate per unit volume:

$$P = \frac{8 \rho}{2 \langle A \rangle H} W \text{ reactions cm}^{-3} \text{ s}^{-1}.\quad (16)$$

Possible interactions with all other nuclei are ignored. The temperature-independent pycnonuclear reaction rate for a bcc lattice, encompassing all the long-range effects of a pycnonuclear reaction, is thus given by

$$P = 8 \frac{\rho A_1 A_2 Z_1^2 Z_2^2}{A_1 + A_2} S(E) \lambda^{7/4} \times \exp\left(\frac{-2.638}{\lambda^{1/2}}\right) (3.90 \times 10^{46} \text{ s}^{-1}), \quad (17)$$

where ρ is in $\text{g}\cdot\text{cm}^{-3}$ and the S-factor is in units of $\text{MeV}\cdot\text{barns}$ [40, 43].

B. Astrophysical S-Factor

The calculations up to this point have started from a macroscopic visualization of the long-range effects. The calculations that follow will invert this viewpoint, instead constructing the astrophysical S-factor from separate models of the different forces with short-range effects. With respect to units in S-factor calculations, the r^* length scale of the bcc lattice is dropped for the more convenient use of fermi. One begins with the total effective potential, the sum of the nuclear and unscreened Coulomb components [41]:

$$V_{\text{eff}}(r, E) = V_{\text{N}}(r, E) + V_{\text{C}}(r) + \frac{l(l+1)\hbar^2}{2\mu r^2}. \quad (18)$$

Since the dominant interaction at the low energies of pycnonuclear reactions is via spherically-symmetric s -wave scattering, l is set to zero in all calculations presented in this effort [40].

The first term, the nuclear potential, is based on one of several methods created in a recent model, referred to in this work as the Sao Paulo model, which was developed by a joint collaboration from several universities and institutes in Brazil [45, 48, 49, 50]. One starts with the concept that the effective one-body interaction between two nuclei can be written schematically as

$$V(\vec{r}, \vec{r}') = V_{\text{bare}}(\vec{r}, \vec{r}') + \sum_i V_i(\vec{r}) G_i(\vec{r}, \vec{r}'; E) V_i(\vec{r}'). \quad (19)$$

The first term on the right is the bare interaction, representing the ground state of an interaction between two nuclei. The second highly-energetic term encompasses polarization and intermediate states, like inelastic channels [48]. This second term is not considered in this effort.

The first term is the focal point of the Sao Paulo model and can be calculated using multiple methods, though the one presented here associates an energy dependence of the derived nuclear potential with nonlocal quantum effects. It begins by concentrating on the effects arising from the Fermi nature of the nucleons. When calculating interaction potentials between nuclei, these effects

translate into a nonlocality. The nonlocality of the bare interaction is solely due to the Pauli exclusion principle, hereafter referred to as Pauli nonlocality [48]. This Sao Paulo methodology creates a local equivalent potential that makes use of a double-folding methodology whereby a representation of the effective nucleon-nucleon force is folded, i.e., integrated, with the densities of the interacting nuclei:

$$V_{\text{bare}} = V_{\text{folding}} = \int \rho_1(r_1) \rho_2(r_2) v_{\text{NN}} d\vec{r}_1 d\vec{r}_2. \quad (20)$$

The result is dependent only on the number of nucleons in the nuclei.

The Sao Paulo group adopts the following form for the bare nuclear potential between two nuclei:

$$V_{\text{bare}}(\vec{r}, \vec{r}') = V_{\text{NL}} \left(\frac{|\vec{r} + \vec{r}'|}{2} \right) \exp \left[-\frac{(\vec{r} - \vec{r}')^2}{b^2} \right], \quad (21)$$

where b is the range of the Pauli nonlocality of the ion-ion interaction [48]. In a sense, this term measures the range of the nonlocal effect where the nuclear force is operative. Jackson and Johnson explain in previous work that

$$b \approx \frac{b_0 m}{\mu} \quad (22)$$

within their single folding model, where b_0 is the nucleon-nucleon nonlocality parameter, m is the nucleon mass, and μ is the reduced mass of the nucleus-nucleus system [51]. Fitting to nucleon-nucleus scattering data, Perey and Buck later show that $b_0 = 0.85 \text{ fm}$ [52]. Continuing to use the density-folding formalism, the nonlocal potential V_{NL} in Eq. (21) is written as [49]

$$V_{\text{NL}} = V_{\text{folding}} = \int \rho_1(r_1) \rho_2(r_2) v_{\text{NN}} d\vec{r}_1 d\vec{r}_2. \quad (23)$$

Using the optical model, the bare nuclear potential is rewritten in terms of a central potential. This requires extracting a local-equivalent potential from a nonlocal expression. A local equivalent potential is defined as [52]

$$\int V(\vec{r}, \vec{r}') \psi_{\text{E}}(\vec{r}') d\vec{r}' \equiv V(\vec{r}, E) \psi_{\text{E}}(\vec{r}). \quad (24)$$

Accordingly, in the central potential notation of the optical model, the total nuclear interaction can be rewritten as [47]

$$\frac{1}{u_l(R)} \int_0^\infty V_l(R, R') u_l(R') = V_{\text{LE}}(R, E) + i W_{\text{LE}}(R, E). \quad (25)$$

As can be seen, there is an energy-dependent, local equivalent potential in the above equation for every term in the effective one-body interaction, with the first term being predominantly real and equivalent to the nonlocal, bare, nuclear interaction while the second term is complex (and

still ignored). In this model, the energy dependence of $V_{\text{LE}}(R, E)$ is chiefly due to Pauli nonlocality in the bare nuclear interaction $V_{\text{bare}}(\vec{r}, \vec{r}')$.

To create this local equivalent potential, the Sao Paulo group uses the Perey and Buck prescription, namely that for a given non-local optical potential depth (V_{NL}), the corresponding local potential depth (V_{LE}) at each energy should be chosen to satisfy the approximate relation

$$V_{\text{LE}} \exp \left[\frac{Mb^2}{2\hbar^2} (E - V_{\text{LE}}) \right] = V_{\text{NL}}, \quad (26)$$

where M is the mass [52]. Using Eq. (21) and recognizing that V_{NL} determines the nonlocal potential depth for the bare nuclear interaction, the local equivalent expression in this case can be written as the following [48]:

$$V_{\text{LE}}(R, E) \approx V_{\text{F}}(R) e^{-\gamma[E - V_{\text{C}}(R) - V_{\text{LE}}(R, E)]}, \quad (27)$$

$$\gamma = \frac{\mu b^2}{2\hbar^2}. \quad (28)$$

This expression has multiple possible interpretations. In one interpretation, the exponent can be tied classically to the kinetic energy E and relative speed v between the nuclei by

$$v^2 = \frac{2}{\mu} E_{\text{K}}(R) = \frac{2}{\mu} [E - V_{\text{C}}(R) - V_{\text{LE}}(R, E)], \quad (29)$$

resulting in

$$\begin{aligned} V_{\text{LE}}(R, E) &\approx V_{\text{F}}(R) e^{-[m_0 b_0 v / 2\hbar]^2} \\ &\approx V_{\text{F}} e^{-4v^2/c^2}, \end{aligned} \quad (30)$$

where c is the speed of light. This interpretation equivalently relates the effect of Pauli nonlocality to that of a velocity-dependent nuclear interaction. In the current work, the local-equivalent potential is instead related directly to the folding potential, which incorporates an effective nucleon-nucleon interaction dependent on the relative speed v between the nucleons [47],

$$V_{\text{LE}}(R, E) = V_{\text{F}} \quad (31)$$

$$V_{\text{F}} = \int \rho_1(r_1) \rho_2(r_2) v_{\text{NN}} \left(v, \vec{R} - \vec{r}_1 + \vec{r}_2 \right) d\vec{r}_1 d\vec{r}_2 \quad (32)$$

$$v_{\text{NN}}(v, \vec{r}) = v_{\text{f}}(\vec{r}) e^{-4v^2/c^2}. \quad (33)$$

This additional modularity allows for different nucleon-nucleon interaction models to be incorporated in future work.

Accordingly, $v_{\text{f}}(\vec{r})$ is the next term to be considered. The Sao Paulo group extrapolated that the effective nucleon-nucleon interaction could be derived by reusing a folding potential from previous heavy-ion potential analyses,

$$v_{\text{f}} = \int \rho_{\text{m}}(r_1) \rho_{\text{m}} V_0 \delta \left(v, \vec{R} - \vec{r}_1 + \vec{r}_2 \right) d\vec{r}_1 d\vec{r}_2, \quad (34)$$

where $V_0 = -456 \text{ MeV fm}^3$. In this scheme, ρ_{m} is the matter density of the nucleon, for which they assumed an exponential shape,

$$\rho_{\text{m}}(r) = \rho_0 e^{-r/a_{\text{m}}}, \quad (35)$$

based on electron scattering experiments that determined the intrinsic charge distribution of the proton in free space. Again, ρ_0 can be determined by the normalization condition from the density calculations [45]. The integration of v_{f} results in a finite-range, nucleon-nucleon interaction,

$$v_{\text{f}} = \frac{V_0}{64\pi a_{\text{m}}^3} e^{-r/a_{\text{m}}} \left(1 + \frac{r}{a_{\text{m}}} + \frac{r^2}{3a_{\text{m}}^2} \right), \quad (36)$$

shown in Fig. 1, where the best-fit value for the matter diffuseness a_{m} of a nucleon is 0.3 fm.

When multiplied by the velocity-dependent exponential in Eq. (33), effects due to Pauli nonlocality are incorporated into this local equivalent, nucleon-nucleon interaction. Unfortunately, with its focus on recreating nonlocal effects, this methodology does not recreate a repulsive core for the nucleon potential, an empirical feature that gives rise to the saturation of the nuclear force. However, this method provides a good fit of heavy-ion potential strengths and is similar to the M3Y potential in the surface region [45].

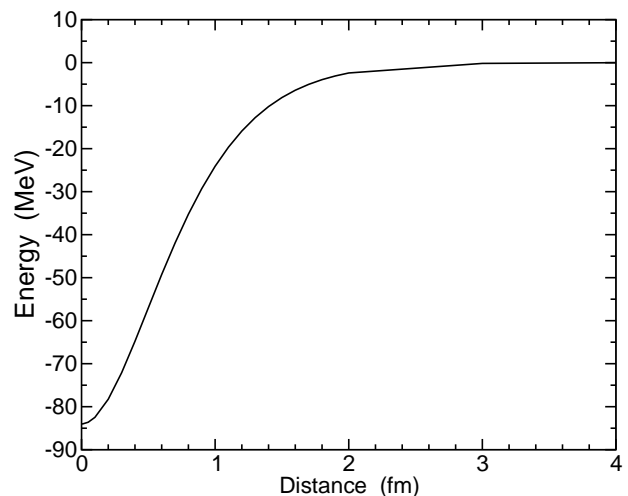


FIG. 1: Nucleon potential without Pauli nonlocality as a function of distance from nuclear center.

The nuclear potential of a system of two C_{12} ions can be seen in Fig. 2. The target ion is considered locked in place near the far-right edge of the graph. The distance between target and projectile centers at the right edge of the graph is greater than the actual distance between the lattice points, i.e., in a two-body picture, the projectile has actually moved past the target; this is the cause of the slight uptick in the nuclear potential.

Moving on from the complications of the nuclear potential, the short-range effects of the Coulomb interaction

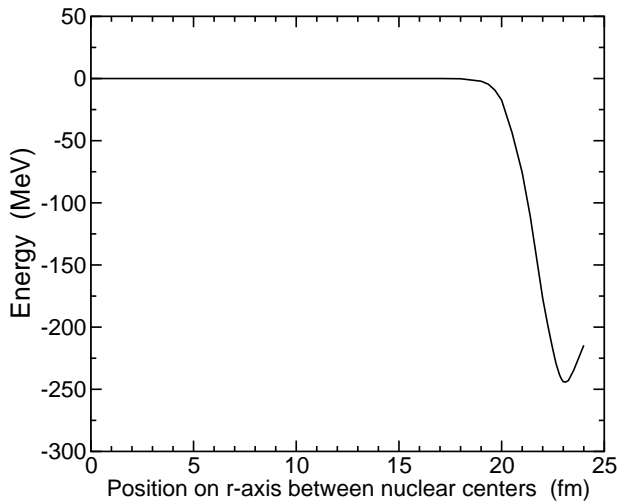


FIG. 2: Nuclear potential between two C_{12} ions as a function of position on the r -axis between nuclear centers for $\rho = 10^{12} \text{ g cm}^{-3}$.

in the effective potential are taken into account. Outside of the nuclei, the point-particle assumption holds. However, in the interior of the nucleus, the expression must be modified to account for the finite size of the nucleus, and the potential energy due to the Coulomb repulsion becomes [48]

$$V_C(r) = \frac{(3R_0^3 - r^3) Z_1 Z_2 e^2}{8\pi\epsilon_0 R_0^3}, \quad r < R_0, \quad (37)$$

within the nucleus.

Having incorporated nuclear and Coulomb interactions into a total effective potential, the calculation of the S-factor is accomplished through the use of a barrier penetration model. This heuristic treatment begins with a calculation of the transmission coefficient through the total effective potential, incorporating this into a model based on fits of thermonuclear data to compute the nuclear cross section [41]. The definition of the S-factor,

$$S(E) \equiv \sigma(E) \times E \times \frac{1}{T}, \quad (38)$$

with the Gamow coefficient T defined for transmission through an unscreened Coulomb barrier, can then be used to calculate the reaction rate.

The transmission coefficient is derived by way of a WKB approximation that requires as input the total effective potential and the total energy. Using the momentum of the reacting system, possible trajectories through the total potential are orthogonal to the surfaces of constant phase of the wavefunction [53]. To solve for the phase, the momentum is integrated between the classical turning points of the effective potential, using

$$\kappa(x) = \frac{1}{\hbar} \{2\mu [V_{\text{eff}}(x) - E_0]\}^{1/2} \quad (39)$$

as the momentum in one dimension [53]. The three-dimensional calculation for phase is then

$$WKB_l = \pm \int_{r_1}^{r_2} \sqrt{\frac{8\mu}{\hbar^2} [V_{\text{eff}}(x) - E_0]} dr. \quad (40)$$

From this, the probability corresponding to the passage of the particle through the effective potential is given by the transmission coefficient

$$T_l = \frac{|\psi_{\text{trans}}|^2}{|\psi_{\text{inc}}|^2} \approx [1 + e^{WKB_l}]^{-1}. \quad (41)$$

In accordance with the barrier penetration model, the fusion cross section is tied to the summation of the total particle flux transmitted through the barrier up to the greatest value of angular momentum in the effective potential [41],

$$\sigma(E) = \frac{\pi\hbar^2}{2\mu E_0} \sum_{l=0}^{l_{\text{cr}}} (2l+1) T_l. \quad (42)$$

The astrophysical S-factor is then calculated by multiplying $\sigma(E)$, the total energy, and the inverse of the transmission coefficient through a pure, unscreened Coulomb barrier.

The fact that the inverse of the Gamow penetration factor is being used is worthy of a second look. The calculations for the total cross section of the reaction have explicitly included a pure Coulomb interaction in the total effective potential. It may seem as if these efforts are being undone by removing the Gamow penetration factor from the S-factor, but this is not the case. The inclusion of the Coulomb interaction in the effective potential was necessary to find the correct turning points for the WKB approximation needed to calculate the total cross section, particularly the turning point for the onset of the nuclear force. But, it is important to remember that the S-factor is supposed to be an expression that compartmentalizes nuclear force effects. Divesting the S-factor of Coulomb forces outside of the nuclear radius follows this paradigm. Furthermore, the reaction rate calculation separately accounts for the effects of the more accurate, *screened* Coulomb potential of the bcc lattice. It is necessary to divide out the traditional, unscreened Gamow penetration factor in order to avoid double-counting Coulomb effects.

C. Atomic Matter Pycnonuclear Reaction Rates

With all of the constituent parts for the calculation in place, pycnonuclear reaction rates for various elements are provided in Figs. 3 and 4 for a range of densities. The reaction rate results for OCP and MCP nuclear matter are a good match to those calculated by the originators of the model, an extended collaboration that included the Sao Paulo group that created the nuclear interaction

methodology and the Joint Institute of Nuclear Astrophysics (JINA) at the University of Notre Dame [43].

At this interim point, the pycnonuclear reaction rates confirm an expected trend. With the data, one can begin to see that the reaction rates decrease as the atomic numbers of the nuclei involved increase. When this methodology is extended to heavy ions that may be found in the inner crust of a neutron star – potentially iron all the way up to neutron drip – the reaction rates continue to plummet, as can be seen by the rapid change in scale for Fig. 4. This makes sense: The increase in the Coulomb repulsion between larger nuclei would make it more difficult to tunnel through the barrier between the ions, even with the effects of Coulomb screening.

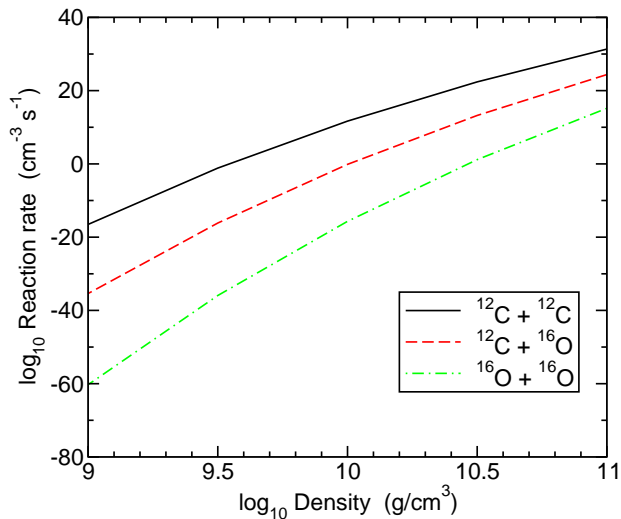


FIG. 3: (Color online) Reaction rates for OCP and MCP atomic matter as a function of density.

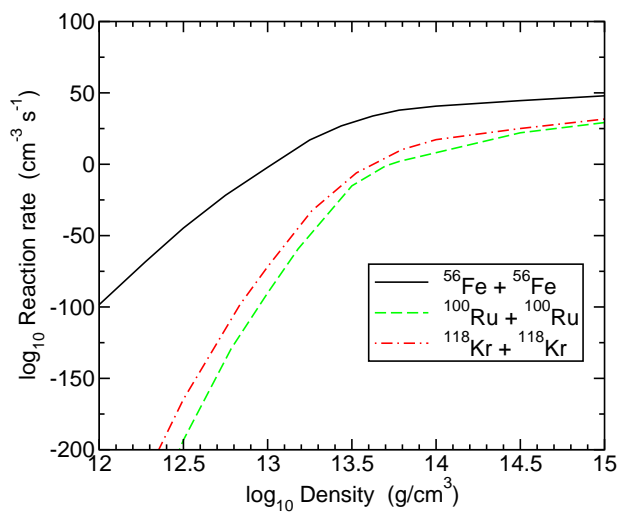


FIG. 4: (Color online) Reaction rates for OCP neutron-rich nuclei as a function of density.

III. STRANGE QUARK MATTER

From here, the effort expands to an attempt at the calculation of pycnonuclear reaction rates between normal nuclear matter and a simple approximation of strange quark matter. It is important to acknowledge immediately that this extension to strange quark matter makes no attempt to modify the methodology of the strong interaction as it has been presented for atomic matter. However, several other models implemented for normal nuclear matter are modified to accommodate theoretical characteristics of strange quark matter, particularly the bulk charge of a strangelet as well as its radius, density, and baryon number. For the purposes of this effort, the term strangelet is used to refer to an approximately nucleus-sized strange quark matter nugget that replaces one of the two normal matter nuclei in the previous reaction calculations.

A. Strangelet Mass

To replace an atomic matter nucleus within the bcc lattice with a strangelet, one needs to know the approximate mass of the strange quark matter nugget. There are numerical studies that have modeled the late stages of in-spiral in binary systems of neutron stars and massive objects such as black holes, white dwarf stars, or other neutron stars. As tidal forces and, eventually, the actual collision overcome the surface tension of strange quark matter and rip the compact objects apart, the release of macroscopic lumps of matter between 10^{-4} and 10^{-1} solar masses, or $A \propto 10^{38}$, seems to be a characteristic feature [54]. It seems a reasonable assumption that a significant fraction of this tidally-released material remains trapped in orbit with typical speeds around $0.1c$ and subject to frequent collisions. If one calculates that the kinetic energy from these collisions is converted to supplying the extra surface and curvature energy necessary for forming smaller strangelets, then the released mass may end up in strangelets with $A \approx 10^2 - 10^3$ [54]. This range is the focus of the input parameters for strange quark matter baryon numbers in the pycnonuclear reaction rate calculations presented below. Since strangelets are self-bound, their mass-radius relationship is given by $M = \int_0^R \epsilon dV \approx 4\pi\epsilon R^3/3$ [25]. Also, instead of using the more rigorous two-parameter Fermi model, the density is assumed to be approximately constant throughout the strangelet.

B. Strangelet Charge

The overall charge of the strangelet is the final parameter changed, and the one that most affects the outcome of the pycnonuclear reaction rates in this study – again, acknowledging that the nuclear interaction is unchanged. We assume that the strangelets are made up of either

ordinary strange quark matter or color superconducting strange quark matter whose condensation pattern is the color-flavor-locked (CFL) phase. Once crucial difference between non-CFL (NCFL) and CFL quark matter is the equality of all quark Fermi momenta in CFL quark matter which leads to charge neutrality in bulk without any need for electrons [55]. This has most important consequences for the charge-to-mass ratios of strangelets. For ordinary strangelets, the charge is approximately

$$Z \approx 0.1 m_{150}^2 A, \quad A \ll 10^3, \quad (43)$$

$$Z \approx 8 m_{150}^2 A^{1/3}, \quad A \gg 10^3, \quad (44)$$

where $m_{150} \equiv m_s/150$ MeV and m_s is the mass of the strange quark. For small A , the charge is the volume quark charge density multiplied by the strangelet volume with a result that is proportional to A itself. This relation holds until the system grows larger than around 5 fm, or $A \approx 150$, at which point the charge is mainly distributed near the strangelet surface, and $Z \propto A^{1/3}$ [56]. In contrast to this, the charge-to-mass ratio of CFL strangelets is described by [56]

$$Z \approx 0.3 m_{150} A^{2/3}. \quad (45)$$

Recently it has been shown that CFL strangelets may even have zero electric charge if the quark pairing is strong [57]. If strangelets should exist in the crusts of neutron stars, this difference may provide a test of color superconductivity.

C. Reaction Rates with Strange Quark Matter

After incorporating these changes due to strange quark matter, pycnonuclear reaction rates between normal nuclear matter and matter nuggets that incorporate some characteristics of strange quark matter are compared in Figs. 5 to 9. In Figs. 5 and 8, the atomic nuclei are paired with strangelets of equivalent baryon number; in Figs. 6 and 9, strangelets of baryon number 500 are used. Previously-shown data for the reaction rates between two atomic matter nuclei are also provided in the graphs for comparison. In these calculations, the strange quark was assumed to have a mass of 300 MeV.

Again looking for possible trends, one can see that the pycnonuclear reaction rates still decrease as the atomic numbers of the nuclei or strangelets involved increase. Additionally, the reaction rates between atomic nuclei and the strange quark matter nuggets are very different than that of normal nuclear matter alone. However, the possibility of a color superconducting state for strange quark matter has dramatic consequences. The extent of the increase in reaction rates when compared to those of atomic nuclei alone is noteworthy, with escalations of over twenty orders of magnitude, at a minimum, at most densities of interest in the cases studied. By comparison,

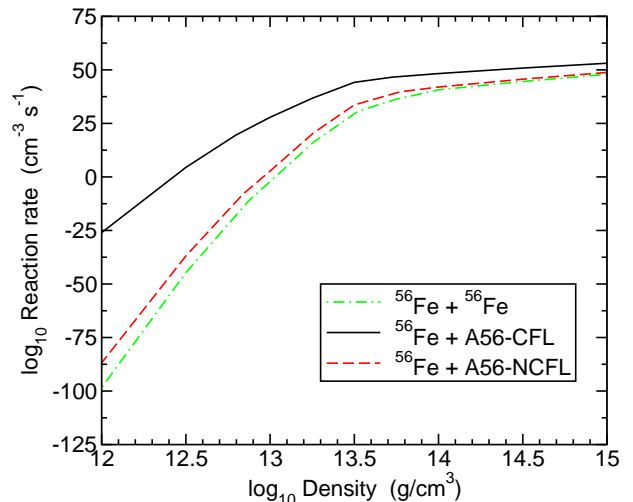


FIG. 5: (Color online) Reaction rates for ^{56}Fe and a strange quark matter nugget with 56 baryons as a function of density.

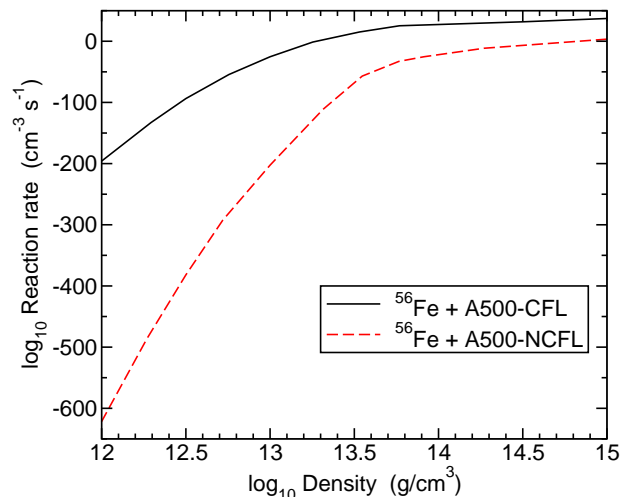


FIG. 6: (Color online) Reaction rates for ^{56}Fe and a strange quark matter nugget with 500 baryons as a function of density.

non-CFL (NCFL) strange quark matter reaction rates are always significantly lower than those of CFL strange quark matter with equivalent baryon number, because of the electric charge difference. The combination of these divergent effects – with CFL and non-CFL strange quark matter rates maintaining a significant gap between them, the inclusion of CFL strange quark matter increasing the reaction rates of atomic nuclei, and increasing baryon number decreasing reaction rates for all systems – makes it difficult to determine *a priori* how reaction rates for a given system will compare to each other.

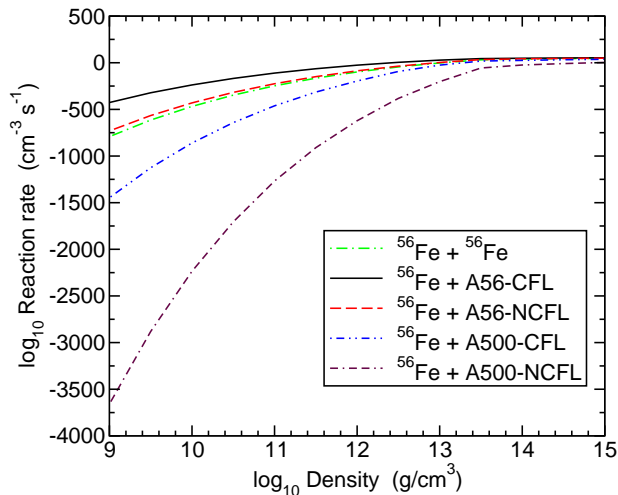


FIG. 7: (Color online) All reaction rates calculated for ^{56}Fe as a function of density.

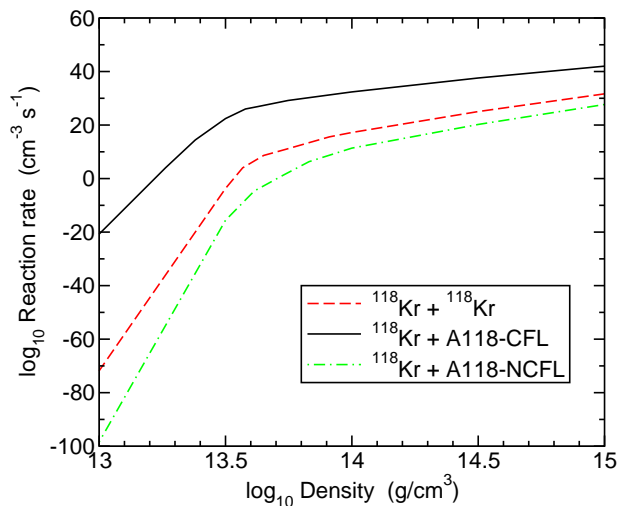


FIG. 8: (Color online) Reaction rates for ^{118}Kr and a strange quark matter nugget with 118 baryons as a function of density.

D. Quark Nugget Concentrations in the Crusts of Neutron Stars

An upper limit on the quark nugget concentration in the crustal regions of neutron stars accreting matter from white dwarfs would be set by the quark nugget flux levels that could have been left over from the Big Bang or from collisions of strange stars [25, 26, 58, 59]. The capture of these quark nuggets by main-sequence stars would be an inevitable consequence of the strange quark matter hypothesis. Due to their large radii, main-sequence stars arise as large-surface long-integration-time detectors for the quark nugget flux [60, 61]. The accreted nuggets should be thermally distributed throughout the interior of main-sequence stars, leading to quark nugget concentrations that would monotonically grow over the lifetime of main-sequence stars. For a constant bath of

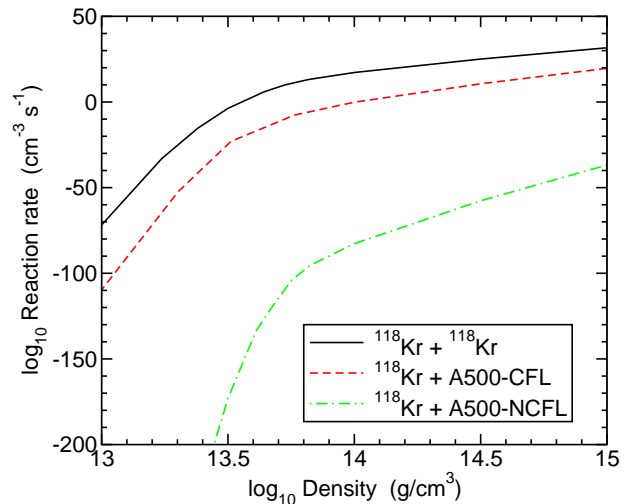


FIG. 9: (Color online) Reaction rates for ^{118}Kr and a strange quark matter nugget with 500 baryons as a function of density.

isotropic monoenergetic quark nuggets, the baryon number accreted onto a main-sequence star can be estimated from [60, 61]

$$A \lesssim 1.6 \times 10^{47} \left(\frac{M}{M_{\odot}} \right)^{-0.15} v_{250}^{-1} \rho_{24} \left(1 + 0.164 v_{250}^2 \left(\frac{M}{M_{\odot}} \right)^{-0.25} \right), \quad (46)$$

where $v_{250} \equiv v_{\infty}/250$ km/s and $\rho_{24} \equiv \rho_{\infty}/10^{-24}$ g/cm³. The quantities v_{∞} and ρ_{∞} denote the quark nugget speed and contribution to the density of the galactic halo far from the star, respectively, and M denotes the mass of a main-sequence star in units of the mass of the sun, M_{\odot} . If one assumes that all the dark matter in the halo of our galaxy would consist of quark nuggets, which is certainly an overestimate, then $\rho_{24} v_{250}^{-1} \sim 1$. Equation (46) then leads for typical progenitor star masses to $A \lesssim 10^{48}$ for the total baryon number of the quark nuggets in white dwarfs, formed from main-sequence stars. This value is to be compared with the typical baryon number of the crust of a neutron star, which is around 10^{54} . Hence, based on this scenario, one would expect less than one quark nugget per 10^6 atomic nuclei. Of course, this ratio may be significantly greater in regions of the Universe (e.g. Globular Clusters) where collisions of strange stars would have generated quark-nugget flux levels that are greatly enhanced in comparison to the homogeneously spread quark-nugget flux level assumed above.

IV. CONCLUSIONS

The methodology presented in this paper provides insight into the magnitude of the rates of pycnonuclear reactions between a simple model of strange quark mat-

ter and atomic nuclei. Recreating a nuclear interaction model and incorporating it in high-density nuclear reaction processes, this effort reconstructs previous calculations for normal nuclear matter. It then expands in scope, extending the model to estimate the changes in the reaction rates as distinctive theoretical characteristics of strange quark matter are substituted for atomic matter.

Assessing the results for all of the data presented, there is an unsurprising decrease in the reaction rates for nuclei with larger atomic numbers, corresponding to the amplification of the Coulomb barrier as the positive charge is increased. In the extended model, though the charge suppression of strangelets was expected to have an effect on pycnonuclear reaction rates, the increase by at least twenty orders of magnitude for reactions between CFL strange quark matter and atomic nuclei at the densities of a neutron star crust was surprising. Reactions that incorporated non-CFL strangelets maintained rates that were significantly lower than the CFL results, another indicator of the additional reduction in charge for the color superconducting system. With these conflicting trends and the associated inability to presciently determine the reaction rates of the differing systems with respect to each other, this methodology for calculating pycnonuclear reaction rates will be of great importance for future astrophysical studies.

As an example, we mention the incorporation of the fusion reaction rates computed in this paper into pycnonuclear reaction fusion network calculations, such as performed by JINA [66]. Such calculations will provide key information about the heat release from neutron stars whose crusts may be contaminated with (superconducting) strange quark matter nuggets. Since the reaction rates of the latter differ by many orders of magnitude from the reaction rates of ordinary nuclear crust matter, nuclear fusion network calculations may have the potential to shed light on the existence of strange quark matter nuggets and on whether or not they are in a color superconducting state, as suggested by QCD [29, 30, 31, 32, 33].

A. Uncertainties

There are several areas of uncertainty. First, the pycnonuclear reaction rate equation in Section II makes use of the WKB integrals J and K , integrals that were numerically calculated for densities between $1.7 \times 10^{-5} \text{g cm}^{-3} \leq \rho / \langle A \rangle A^3 Z^6 \leq 1.7 \times 10^4 \text{g cm}^{-3}$ [40]. The densities possible from the outer crust to the core of a neutron star are all several orders of magnitude greater than this density range. In the attempt to recreate previous efforts that used and did not change the pycnonuclear reaction rate equation, the applicability of the Salpeter and Van Horn calculation at these densities has been assumed.

There is also the issue of the nuclear potential model

for atomic matter. Referring again to Fig. 1, it should be noted that the Sao Paulo model does not implement a repulsive, hard core for the nuclear interaction. Given its focus on recreating nonlocal effects with a local-equivalent potential, it is quite possible that it was never intended to do so. Though it shows similarities to the M3Y potential in the surface region of nuclei and provides a good fit to data of heavy-ion potential strengths [45], its validity has been called into question [62, 63]. It is also critical to remember that this study leaves the nuclear interaction model unchanged when the adjustments for strange quark matter are made. Any possible conclusions must be weighed against this deficiency.

B. Future Work

There are several avenues available for future work. The initial suggestions begin with the known sources of error just mentioned in Sect. IV A. Though any analysis and modification of the J and K WKB integrals for the pycnonuclear reaction rate equation is a task heavily steeped in numerical and complex analysis, Salpeter and Van Horn do offer many details about their calculations in their published work [40, 64]. A verification that the current reaction rate equation properly accounts for the densities under consideration in a neutron star would be of use.

There is another opportunity in that the modularity of this methodology allows for comparisons of different nuclear force models. If one does not intend to model exotic matter, the current methodology may still be used to assess changes in reaction rates due to various nuclear interaction models. It may be possible that such comparisons may provide support for the use of one nuclear model over another.

Future efforts may include an improved model of the nuclear interaction with strange quark matter. The current double-folding process that determines the total nuclear potential uses a model of the nuclear force that is assumed to be applicable to both the target and projectile nuclei within the lattice. If a strangelet interaction model is included, future efforts may need to alter the subordinate nuclear potential v_{NN} prior to its integration with the strangelet and atomic matter densities. On the other hand, a simpler analysis could focus on any effects of the reaction rates that may stem from changing the mass of a strange quark, assumed to be 300 MeV, within the current strange quark matter model.

Separately, it may also be useful to assess the effect of strangelets or different atomic nuclei on the pycnonuclear reaction rates of nearby interacting particle pairs. This sort of calculation, focused on the effects of lattice imperfections, has not been extensively studied even for normal nuclear matter. This is not a three-body calculation, since the environment already contains many nearby particles frozen in a lattice. The lattice imperfection would first alter the geometry of the electrostatic screening po-

tential in Section II, affecting the vibrational energy levels of a nearby interacting ion pair and, in turn, influencing the reaction rate. Since the screened Coulomb potential is also used to determine the wavefunction of the incoming particle, it is likely that this particular line of research would require extensive changes to the pycnonuclear reaction rate equation itself. The methodology for the calculation of the S-factor could remain unchanged.

In addition, follow-on efforts may wish to incorporate pycnonuclear reaction rates into stellar thermal models, possibly flowing potential characteristics of strange quark matter to observable predictions. As a first approximation, the zero-temperature pycnonuclear reaction rate was used in this effort; future efforts may wish to incorporate the temperature-dependent pycnonuclear reaction rate equation developed by Salpeter and Van Horn [40]. One could build on this by calculating an energy generation rate in units of $\text{erg g}^{-1} \text{s}^{-1}$ that can be obtained by multiplying the pycnonuclear reaction rate equation by $Q/2\rho$ [40]. Q is the energy release in a single reaction. Approximations for Q would need to be made for strange quark matter, perhaps building on estimates that the to-

tal energy release for normal nuclear matter is 1.45 MeV per baryon [65]. These thermal calculations could then be incorporated into stellar heating models, evaluating possible variations in total heat output for neutron stars due to normal matter or strangelets that may be present as a result of state changes or accretion. Differences in reaction rates may thus provide a clue to the presence of strange quark matter in astrophysical environments.

In any case, it is hoped that this investigation may serve as a stepping stone for further studies, and that these future possibilities may tie astrophysical observations of high-density objects to speculations about the possible existence of (color superconducting) strange quark matter.

Acknowledgments

This work was supported by the National Science Foundation (USA) under Grant PHY-0457329.

-
- [1] N.K. Glendenning, *Compact Stars, Nuclear Physics, Particle Physics, and General Relativity*, Springer-Verlag, New York, 2000.
 - [2] F. Weber, *Pulsars as Astrophysical Laboratories for Nuclear and Particle Physics*, High Energy Physics, Cosmology and Gravitation Series, IOP Publishing, Bristol, Great Britain, 1999.
 - [3] D.D. Ivanenko and D.F. Kurdgelaidze, *Astrophys. J.* **1**, 251 (1965).
 - [4] H. Fritzsche, M. Gell-Mann, and H. Leutwyler, *Phys. Lett.* **47B**, 365 (1973).
 - [5] G. Baym and S.Chin, *Phys. Lett.* **62B**, 241 (1976).
 - [6] B.D. Keister and L.S. Kisslinger, *Phys. Lett.* **64B**, 117 (1976).
 - [7] G. Chapline and M. Nauenberg, *Phys. Rev. D* **16**, 450 (1977); *Ann. New York Academy of Sci.* **302**, 191 (1977).
 - [8] W.B. Fechner and P.C. Joss, *Nature* **274**, 347 (1978).
 - [9] N.K. Glendenning, *Phys. Rev. D* **46**, 1274 (1992) 1274.
 - [10] M. Alford, D. Blaschke, A. Drago, T. Klähn, G. Pagliara, and J. Schaffner-Bielich, *Nature* **445**, 7 (2007).
 - [11] D.B. Kaplan and A.E. Nelson, *Phys. Lett.* **175B**, 57 (1986); *ibid.* *Nucl. Phys.* **A479**, 273 (1988).
 - [12] G.E. Brown, K. Kubodera, and M. Rho, *Phys. Lett.* **192B**, 273 (1987).
 - [13] G.E. Brown, *Kaon condensation in dense matter*, in: *Bose-Einstein Condensation*, ed. A. Griffin, D. W. Snoke, and S. Stringari, Cambridge Univ. Press, 1995, p. 438.
 - [14] G.Q. Li, C.-H. Lee, and G.E. Brown, *Nucl. Phys.* **A625**, 372 (1997); *ibid.* *Phys. Rev. Lett.* **79** (1997) 5214.
 - [15] G.E. Brown, *Phys. Bl.* **53**, 671 (1997).
 - [16] J.M. Lattimer and M. Prakash, *Astrophys. J.* **550**, 426 (2001).
 - [17] F. Weber, *Progress in Particle and Nuclear Physics* **54**, 193 (2005).
 - [18] T. Klähn *et al.*, *Phys. Rev. C* **74**, 035802 (2006).
 - [19] A. Sedrakian, *Prog. Part. Nucl. Phys.* **58**, 168 (2007).
 - [20] D. Page and S. Reddy, *Ann. Rev. Nucl. Part. Sci.* **56**, 327 (2006).
 - [21] E. Farhi and R. Jaffe, *Phys. Rev. D* **30**, 2379 (1984).
 - [22] J. Schaffner-Bielich, C. Greiner, A. Diener, and H. Stoecker, *Phys. Rev. C* **55**, 3038 (1997).
 - [23] C. Alcock, E. Farhi, and A. Olinto, *Astrophys. J.* **310**, 261 (1986).
 - [24] C. Alcock and A. V. Olinto, *Ann. Rev. Nucl. Part. Sci.* **38**, 161 (1988).
 - [25] J. Madsen, *Lecture Notes in Physics* **516**, 162 (1999).
 - [26] E. Witten, *Phys. Rev. D* **4**, 272 (1984).
 - [27] A.R. Bodmer, *Phys. Rev. D* **4**, 1601 (1971).
 - [28] H. Terazawa, *INS-Report-338* (INS, Univ. of Toyko, 1979); *J. Phys. Soc. Japan*, **58**, 3555 (1989); *ibid.* **58**, 4388 (1989); *ibid.* **59**, 1199 (1990).
 - [29] K. Rajagopal, F. Wilczek, in: M. Shifman (Ed.), *The Condensed Matter Physics of QCD, At the Frontier of Particle Physics/Handbook of QCD*, World Scientific, 2001.
 - [30] M. Alford, K. Rajagopal, and F. Wilczek, *Phys. Lett.* **422B**, 247 (1998).
 - [31] M. Alford, *Ann. Rev. Nucl. Part. Sci.* **51**, 131 (2001).
 - [32] R. Rapp, T. Schäfer, E.V. Shuryak, and M. Velkovsky, *Phys. Rev. Lett.* **81**, 53 (1998); *ibid.* *Ann. Phys.* **280**, 35 (2000).
 - [33] M.G. Alford, A. Schmitt, K. Rajagopal, and T. Schäfer, *Rev. Mod. Phys.* **80**, 1455 (2008).
 - [34] M.S. Berger and R.L. Jaffe, *Phys. Rev. C* **35**, 213 (1987).
 - [35] J. Schaffner, C. Greiner, and H. Stöcker, *Phys. Rev. C* **46**, 322 (1992).
 - [36] E.P. Gilson and R.L. Jaffe, *Phys. Rev. Lett.* **71**, 332 (1993).
 - [37] Y. Zhang and R.-K. Su, *Phys. Rev. C* **67**, (2003) 015202.
 - [38] R.E. Peierls, *Quantum Theory of Solids*, Oxford Univer-

- sity Press, Oxford, 2001.
- [39] S.L. Shapiro and S.A. Teukolsky, *Black Holes, White Dwarfs, and Neutron Stars*. John Wiley & Sons, Inc., New York, 1983.
- [40] E.E. Salpeter and H.M. Van Horn, *Astrophys. J.* **155**, 183 (1969).
- [41] L.R. Gasques, A.V. Afanasjev, E.F. Aguilera, M. Beard, L.C. Chamon, P. Ring, M. Wiescher, and D.G. Yakovlev, *Phys. Rev. C* **72**, 025806 (2005).
- [42] D.D. Clayton, *Principles of Stellar Evolution and Nucleosynthesis*, University of Chicago Press, Chicago, 1983.
- [43] D.G. Yakovlev, L.R. Gasques, A.V. Afanasjev, M. Beard, and M. Wiescher, *Phys. Rev. C* **74**, 035803 (2006).
- [44] W.J. Carr, Jr., *Phys. Rev.* **122**, 1437 (1961).
- [45] L.C. Chamon, B.V. Carlson, L.R. Gasques, D. Pereira, C. De Conti, M.A.G. Alvarez, M.S. Hussein, M.A.C. Ribeiro, E.S. Rossi, Jr., and C.P. Silva, *Phys. Rev. C* **66**, 014610 (2002).
- [46] L.R. Gasques, L.C. Chamon, D. Pereira, M.A.G. Alvarez, E.S. Rossi, Jr., C.P. Silva, and B.V. Carlson, *Phys. Rev. C* **69**, 034603 (2004).
- [47] L.C. Chamon, B.V. Carlson, L.R. Gasques, D. Pereira, C. De Conti, M.A.G. Alvarez, M.S. Hussein, M.A.C. Ribeiro, E.S. Rossi, Jr., and C.P. Silva, *Brazilian Journal of Physics* **32**, 238 (2003).
- [48] M.A.C. Ribeiro, L.C. Chamon, D. Pereira, M.S. Hussein, and D. Galetti, *Phys. Rev. Lett.* **78**, 3270 (1997).
- [49] L.C. Chamon, D. Pereira, M.S. Hussein, M.A.C. Ribeiro, and D. Galetti, *Phys. Rev. Lett.* **79**, 5218 (1997).
- [50] L.C. Chamon, D. Pereira, and M.S. Hussein, *Phys. Rev. C* **58**, 576 (1998).
- [51] D.F. Jackson and R.C. Johnson, *Phys. Lett.* **49B**, 249 (1974).
- [52] F. Perey and B. Buck, *Nucl. Phys.* **32**, 253 (1962).
- [53] L.I. Schiff, *Quantum Mechanics*, 3rd ed. McGraw-Hill, New York, 1968.
- [54] J. Madsen, *J. Phys.* **G28**, 1737 (2002).
- [55] K. Rajagopal and F. Wilczek, *Phys. Rev. Lett.* **86**, 3492 (2001).
- [56] J. Madsen, *Phys. Rev. Lett.* **87**, 172003 (2001).
- [57] M. Oertel and M. Urban, *Phys. Rev. D* **77**, 074015 (2008).
- [58] S.J. Cho, K.S. Lee, and U. Heinz, *Phys. Rev. D* **50**, 4771 (1994).
- [59] W. N. Cottingham, D. Kalafatis, and R. Vinh Mau, *Phys. Rev. Lett.* **73**, 1328 (1994).
- [60] J. Madsen, *Phys. Rev. Lett.* **61**, 2909 (1988).
- [61] J. Madsen, *Quark Nuggets, Dark Matter and Pulsar Glitches*, Proc. of the XXIVth Rencontre de Moriond, Les Arcs, Savole, France, March 5–12, 1989, ed. by J. Audouze and J. Tran Thanh Van (Edition Frontiers, 1990).
- [62] S. Misicu and H. Esbensen, *Phys. Rev. C* **75**, 034606 (2007).
- [63] L.R. Gasques, E. Brown, A. Chieffi, C.L. Jiang, M. Limongi, C. Rolfs, M. Wiescher, and D. G. Yakovlev, *Phys. Rev. C* **76**, 035802 (2007).
- [64] H.M. Van Horn and E.E. Salpeter, *Phys. Rev.* **157**, 751 (1967).
- [65] D.G. Yakovlev, K.P. Levenfish, and O.Y. Gnedin, *Eur. Phys. J.* **A25**, 669 (2005).
- [66] Information about JINA can be found at www.jinaweb.org.